Wiese, B., Böhner, J., Enachescu, C., Würdemann, H., Zimmermann, G. (2010): Hydraulic characterisation of the Stuttgart formation at the pilot test site for CO2 storage, Ketzin, Germany. - International Journal of Greenhouse Gas Control, 4, 6, 960-971

DOI: 10.1016/j.ijggc.2010.06.013

Hydraulic characterisation of the Stuttgart formation at the pilot test site for CO2 storage, Ketzin, Germany

Bernd Wiese[1a], Jörg Böhner[2], Cristian Enachescu[2], Hilke Würdemann[1], Günter Zimmermann[1]
1= GFZ Helmholtz Centre Potsdam GFZ German Research Centre for Geosciences, Centre for CO_2 Storage, Telegrafenberg, D-14473 Potsdam, Germany
2= Golder Associates GmbH, Vorbruch 3, D-29227 Celle, Germany

a = corresponding author. Tel +49 331 288-1823; Fax: +49 331 288-1529 Email: wiese@gfz-potsdam.de

Abstract

The paper presents an approach for the interpretation of hydraulic tests of a CO_2 storage reservoir. The sandstone reservoir is characterised by a fluviatile channel structure embedded in a low-permeability matrix. Pumping tests were carried out in three wells, with simultaneous pressure monitoring in each well.
The hydraulic parameters (permeability and storativity) and the boundary configurations were calibrated using three different approaches: (i) parameter calibration and type curve interpretation for single-hole tests, (ii) calibration of the entire build-up phase for cross-hole tests, and (iii) calibration of the initial pressure response for cross-hole pumping tests. In addition, the arrival time of the pressure response was determined and provides additional information about the pathways of hydraulic connection.
The measured pumping test permeabilities of the formation were much lower than those measured on the cores, which is very unusual. The pumping test permeabilities are mainly between 50 and 100 millidarcy (mD), while core samples show a mean aquifer permeability of 500 to 1,100 mD. Based on this it was concluded that some kind of continuous low permeability structure exists, which was supported by core material. Three possible aquifer configurations were considered. The first and second were derived from traditional pumping test analysis and were conceptualised using flow boundaries. Each of the analyses provides a different result. A method was developed in which these differences were resolved by interpreting the pressure response with respect to its spatial and temporal sensitivity. This solution lead to a third configuration which was mainly based on spatially-variable permeabilities. Taking into account the pumping test results, the geological background and the behaviour of injected CO_2, we consider only the third configuration to be realistic. The results are in good agreement with modelled CO_2 arrival times and pressure history.

Keywords: Ketzin, pumping test, cross-hole, permeability, core, response time, CO_2 storage, spatial, temporal, sensitivity

1 Introduction

In this paper, we present an approach for the pre-injection hydraulic characterisation of a CO_2 storage reservoir. Flow and transport modelling of CO_2 requires knowledge of the (saturated) hydraulic permeability on a field scale. It is directly relevant to the flow of the replaced saline pore water. It also determines the order of magnitude of unsaturated permeability, since the impact of the uncertainty of the relative permeability is smaller than the impact of the uncertainty of the saturated permeability.
The objectives of the present investigation were to provide field-scale values of the hydraulic permeability and information about the aquifer configuration and impermeable flow boundaries. We have determined pumping test-derived values and have compared them to core permeabilities, both of which may differ significantly (Hart et al. 2006, Urban and Gburek 1988, Worthington 1977, Renard et al. 2006).

The storage formation at the Ketzin site is the so-called Stuttgart Formation, which was formed by alluvial processes and exhibits a very heterogeneous lithology. The aquifer is composed of high-permeability sandstone channel facies of good reservoir quality alternating with floodplain mudstone facies of poor reservoir quality (Förster et al. 2006). The distribution of the sandstone within the mudstone matrix is highly heterogeneous on a regional scale and therefore cannot be easily predicted (Frykman et al. 2006). Three boreholes (CO2 Ktzi 200/2007, CO2 Ktzi 201/2007, CO2 Ktzi 202/2007, in the following referred to without the prefix and suffix), which are completed as wells, are located in the area of investigation (Prevedel et al., 2008). The inter-borehole distance is between 50 and 112 m.

A cross-hole pumping test was carried out in each of the three wells (Ktzi 200, Ktzi 201 and Ktzi 202). The test setup had to comply with several objectives (Würdemann et al. 2010) and could therefore not be optimised for hydraulic interpretation (see 2.2, Test description). The objectives of the tests were as follows:

- To remove the process fluids from the drilling and other operations (drillmud, viscous pill), in order to prepare the wells for the future CO_2 injection and observation
- To procure formation water samples
- To identify the near-well conditions (productivity, skin factor)
- To evaluate the tests used to derive hydraulic parameters of the aquifer

All of the tests presented here are pumping tests. Other hydraulic tests, such as nitrogen lifts (Zettlitzer et al. 2010) and injection tests, have also been carried out at this test site, but were not analysed here.

The hydraulic parameters were calibrated using three different approaches: (i) parameter calibration by type curve interpretation of single-hole tests, (ii) calibration of the cross-hole pumping test pressure history, and (iii) calibration of the initial pressure response to the cross-hole pumping test. In addition, the arrival time of the pressure response was determined, and provides rather unambiguous information about hydraulic conductivity and connection pathways. As result of (i) and (ii), we obtained the hydraulic permeabilities and configurations of boundary conditions. Both approaches require the assumption of a homogeneous aquifer. However, the hydraulic parameters show significant differences in space, disproving the assumption of homogeneity. This contradiction was resolved by using the additional results from approach (iii) and interpreting them with consideration to spatially and temporally-dependent sensitivities (Leven et al. 2006, Vasco et al. 2000). The parameters identified in this manner were attributed to the area for which the method provided the most sensitive results. In this context, it must be considered that heterogeneous parameter distributions may provide the image of a rather homogeneous aquifer with calibrated hydraulic parameters representing a mean value. This is of particular relevance for cross-hole pumping tests, since the sign of the sensitivity varies in space, and the magnitude and most sensitive regions vary in time (Leven et al. 2006). While type curve analysis is an established method for pumping test evaluation, the authors are not aware of publications which consider spatial and temporal sensitivities for a comprehensive interpretation. The present approach is an intermediate step between traditional pumping test interpretation and inverse modelling and allows us to resolve part of the natural heterogeneity.

The results are discussed with respect to field observations of CO_2 arrival at the observation wells (Kempka et al., 2010) and the results of history matching of the injection pressure at Ktzi 201 (Lengler et al., 2010).

2 Material and Methods

2.1 Geology and Boreholes

The test-site is located within the Roscow-Ketzin anticline. Data from eight boreholes provide background information on the lithology and petrophysics, and the entire formation has been described by Förster et al. (2006). The test-site is located on the flank of the Ketzin part, for

which a 3D regional seismic campaign was carried out (Juhlin et al. 2007). The campaign showed no evidence of fractures in the vicinity of the wells.
The storage reservoir is part of the Stuttgart formation, which has a depth between 610 m b.g.l. and 730 m b.g.l. at the present location. The formation consists of two main compartments, which are sandstone channels embedded in mudstone (Förster et al. 2006). The observed thicknesses of the main sandstone formations are 5 m to 15 m. According to Förster et al. (2006), these thicknesses are expected to correlate to a channel width between 100 m and 1600 m. The distribution of mud- and sandstone cannot be well predicted (Frykman 2006).
The wells Ktzi 200, Ktzi 201 and Ktzi 202 form a right-angled triangle with leg lengths of 50 m and 100 m. At these wells, the sandstone is divided into aquifer layers with thicknesses of 5 m to 8 m (Figure 1). The core analyses and borehole logs show an effective aquifer porosity of about 20% (Norden et al. 2010). The layer's average horizontal core permeabilities range between 500 mD and 1,100 mD (Table 1). The upper and lower compartments show a permeabilities of 500 mD and1300 mD, respectively (Förster et al, submitted). Thin layers of sandstone and siltstone exist below the main aquifers (Figure 1). They belong to overbank facies and are probably not connected to the flow system (Förster et al, submitted).The mudstone shows a permeability in the microdarcy range (Norden et al. 2010).
Although the distribution of the sandstone is not well-predicted on the regional scale (Frykman 2006), the sandstone structure in Ktzi 200 and Ktzi 201 is very similar, suggesting that they belong to the same channel (Norden et al., personal communication). The sandstone thickness in Ktzi 202 is reduced and its elevation is a few meters higher, following the dip of the anticline. From geological information alone, it is not possible to judge whether the sandstone in Ktzi 202 is part of the same channel (Norden, personal communication). We therefore assume that the well tube is not in hydraulic contact with the entire profile. Part of the annular space is cemented (Figure 1), but the thin sand- and siltstone layers which are connected to the non-cemented part may contribute to the hydraulic behaviour. Nevertheless, the potential flow contribution is small. We conclude as working hypothesis for the pumping test type curve interpretation that the storage reservoir can be approximated as horizontal aquifer.

2.2 Test description

Pumping tests were carried out in each of the three wells between September 2007 and January 2008. Due to budgetary considerations, the tests duration had to be minimised (Table 2). Since the tests had to comply with several objectives, they were not optimised for hydraulic testing. The tests were conducted without packers, as all fluid from the borehole had to be removed and replaced with formation water. As a consequence, the wellbore storage was high and pumping rates were significantly higher during the first few minutes (70 to 250 l min^{-1}), until the well pressure stabilised. The pumping tests were carried out with the maximum pumping rate with respect to the allowable drawdown. The pumping rates were between 1.1 m^3 h^{-1} and 1.8 m^3 h^{-1} (Table 2), which was much lower than expected from the core permeabilities.

2.3 Instrumentation

Two pressure transducers were installed in the pumping wells. The upper transducer (type: Aquitronic) was fixed to the pump and allowed online monitoring during test operation. The lower transducer (type: Spartek) was installed close to the well screen and provided high resolution data, which are evaluated here.
As an example, the design for the pumping test in well Ktzi 201, which differs from the others only in terms of transducer and pump elevations, is presented in Figure 2. The observation wells were each equipped with one pressure transducer (type: Aquitronic or Weatherford) which were installed about 5 m to 15 m below the water table.

2.4 Data evaluation

The aquifer was simulated as a single layer homogeneous porous aquifer with single phase flow. The pressure drawdown in an aquifer caused by a pumping well is described by:

$$\frac{\partial^2 s}{\partial r^2} + \frac{1}{r}\frac{\partial s}{\partial r} = \frac{S}{T}\frac{\partial s}{\partial t} \quad \textbf{Eq. (1)}$$

where r is the distance to the pumping well [m], s is the drawdown pressure height [m], S is the coefficient of storage [-] t is the time [s] and T is the transmissivity [m² s^{-1}]. The hydraulic head can be converted to pressure using the fluid density. The transmissivity is converted to permeability, k [m²], using Eq. (2):

$$k = T\,\eta\,\rho^{-1}\,g^{-1}\,h^{-1} \quad \textbf{Eq. (2)}$$

where η [Pa s] is the dynamic viscosity, ρ [kg/m³] is the fluid density in the well, g [m s^{-2}] is the gravitational acceleration and h [m] is the aquifer thickness. The reservoir fluid is NaCl dominated, with 235 g/l total dissolved solids and less than 10 g/l of the secondary constituents SO_4^{2-} and Fe^{2+} (Würdemann et al. 2010). At a temperature of 32°C to 34°C, the value of η is equal to 1.2 10^{-3} Pa s. The pumping test evaluation provides values for transmissivities, but for readability we also present the derived permeabilities. They comprise some degree of uncertainty, since the aquifer thickness is not exactly known. The fluid density and viscosity can be approximated. We specify the permeability in millidarcy [mD], with 1 mD = 9.87 10^{-16} m².

The software package Interpret2006 (Paradigm 2006) was used to evaluate the pumping tests. Interpret2006 uses a constant rate solution to provide optimised hydraulic parameters for a wide range of potential reservoir models. It can be applied to calculate the superposition of constant rate events, non-linear regression and multi-event rate normalised plots. In the current evaluation, the aquifer was modelled as a homogeneous formation, intersected by up to two linear impermeable hydraulic boundaries. The fitting parameters of the single hole evaluation were aquifer transmissivity, wellbore skin factor, equilibrated formation pressure, wellbore storage, distance to impermeable boundaries, and in cases with more than one boundary, the angle between them. The calibration procedure of the observation wells allowed the incorporation of a maximum of one boundary condition with a defined position relative to the pumping and observation wells. The calibration procedure also included the aquifer storage coefficient, but did not include the wellbore storage and skin, since the Interpret2006 uses a line source model for cross-hole tests.

Several methods exist for the identification of spatial structures and variability (e.g. Vasco et al. 2000, Vasco et al. 2001, Li et al. 2007, Wiese and Nützmann 2008). However, these approaches were designed to analyse large datasets and do not permit the evaluation of single-hole tests. In this study, we cannot disregard the single-hole tests, and the small size of our dataset both allows for and requires a manual interpretation of sensitivities. We have therefore combined the type curve evaluation in the pumping well with matching the entire build-up phase in the observation wells. The authors are not aware of any previous studies in which this methodology of considering sensitivities has been applied to a test-site.

For single hole tests, permeable and impermeable boundaries produce characteristic shapes in the drawdown type curves (e.g., Zambrano et al. 2000, Bourdet 2002). However, interpretation implies non-uniqueness, i.e., different spatially inhomogeneous conductivities may produce similar type curves. Particularly short type curves without a characteristic shape are susceptible to non-uniqueness (Daungkaew et al. 2000), and require a careful interpretation with respect to the types of heterogeneities and their distance to the well. Single-hole tests have radially-symmetric negative sensitivity, in which the sensitive area increases with time (Leven et al. 2006). The time period can therefore be used to estimate the distance to heterogeneities and the radius of investigation R [m], with t as the time and S as the storage coefficient (e.g. Streltsova 1987, Eq. (3)). Compared to approaches

reviewed in Daungkaew et al. (2000), the approach applied here estimates a lower radius of investigation. The direction of heterogeneities cannot be determined with a single hole test.

$$R = 2\sqrt{\frac{T\,t}{S}} \qquad \textbf{Eq. (3)}$$

Cross-hole observations provide additional information about aquifer parameters, including their spatial distributions and directions. The results are analysed with transmissivity-normalised plots (Enachescu et al. 2004).

However, compared to single-hole tests, the interpretation is more difficult, because the results have a higher degree of non-uniqueness. In the case of transmissivity, these observations have regions of positive and negative sensitivity (Leven et al. 2006). While a positive correlation between drawdown and transmissivity exists within a circular area between the observation wells, outside the circle the sensitivity is negative (Figure 3). In cross-hole tests, storativity shows the highest sensitivity near to the pumping and observation wells, without undergoing a change in sign (Vasco et al. 2000). However, this property is frequently subject to overfitting due to variations in unresolved, small scale transmissivity (Li et al. 2007, Wiese and Nützmann 2008). Furthermore, for initial pressure calibration, permeability and storativity show a higher cross-correlation than for the fitting of the entire build-up phase.

Unlike for single-hole tests, where evaluation of very early data is inhibited by the wellbore storage and the skin effect, these effects are negligible for cross-hole tests in the observation well. Therefore, the initial pressure response can be evaluated, and its sensitivity is particularly relevant. Initially, cross-hole tests are most sensitive to the region within a circle between the pumping and observation wells (Leven et al. 2006, Figure 3). With increasing duration, the sensitivity is shifted to areas further away from the circle and can be used for characterisation of more distant points in the aquifer (e.g. Vasco et al. 2000, Leven et al. 2006). The sensitivity of the initial behaviour is small compared to the sensitivity of later data. In order to extract results that are targeted to the region between the wells, we evaluate the earliest clear signal separately, which requires the highest possible derivative of the pressure response. For real data showing noise and limited resolution, we find the first derivative to be appropriate. Determining aquifer parameters separately, and using early and late information from the pumping test, allows us to distinguish the aquifer parameters between the two observation wells from more distal regions. We have therefore calibrated the transmissivity and storage coefficient separately using the initial pressure response.

We consider it very useful to include the response time in the observation wells. The time is determined by identifying the initial pressure response of the first pressure derivation, (dp/dt). By using the reaction time, it is possible to estimate the distance of the hydraulic connection between the wells and unambiguously reject hypotheses in which no-flow boundaries cause deviations from the direct connection.

3 Results and Discussion

3.1 Pumping well type curves

The type curve analysis provided transmissivity results for the area around the tested well. The fitting parameters for this analysis were aquifer transmissivity, wellbore skin factor, equilibrated formation pressure, wellbore storage, distance of impermeable boundaries, and in cases with more than one boundary, the angle between them. Several configurations, with and without no-flow boundaries, were modelled. The modelled type curve data show a very good fit to the observed data, which are both presented in Figure 4 to Figure 6. All type curves exhibit a rounded peak just prior to about one hour of elapsed time, indicating a pronounced wellbore storage effect and a positive skin. Both effects cover the aquifer response in the immediate vicinity of the well, i.e., within a radius of about 50 m. According to Eq. (3), the radius of investigation is about 220 m.

For the well Ktzi 200, the pressure derivative type curve (Figure 4) begins to increase after three hours of elapsed time. This indicates that the permeability decreases with increasing distance from the well. We may reasonably assume that a no-flow boundary is present, which was calibrated at a distance of 39 m. However, the boundary is quite close to the observation well, such that it cannot be distinguished explicitly from near wellbore effects. Therefore, other configurations with decreasing radial permeability may also be responsible for the measured signal.

For the well Ktzi 201, the derivative begins to increase after 10 hours, with a steeper slope than for Ktzi 200. The magnitude of the slope clearly suggests the presence of a no-flow boundary, which is calibrated in a distance of 134 m. However, the slope is larger than that expected from a single boundary, so we used a second boundary which is calibrated in a distance of 29 m. However, as with Ktzi 200, the latter boundary cannot be clearly distinguished from near wellbore effects.

For the well Ktzi 202, the derivative decreases continuously with increasing distance from the well. The type curve does not provide any indication of flow boundary conditions in the area around the bore hole. However, without a no-flow boundary, the permeability is 54 mD, which is lower than the values from the other wells. If an impermeable boundary existed close to the well (5 - 10 m), the permeabilities would be twice as high. However, this hypothesis would require a skin factor value of five, which is not unrealistic, but is higher than for the other wells (Table 3; Figure 6). We conclude that the no-boundary configuration is more likely. The analytical solutions have provided information with respect to the presence of flow boundaries, but the results are non-unique and the model assumption of infinite boundary length and homogeneous aquifer conditions do not allow for a consistent interpretation. For example, for Ktzi 201, the single hole interpretation suggests the existence of two boundaries, while for the cross-hole tests one boundary appears appropriate. The distance of the nearest boundary to Ktzi 201 varies between 8 m and 95 m (Table 3). For Ktzi 200, the boundary distances are between 29 m and 79 m, and when mapped, are shown to have a different angle (Table 3). Even when considering a finite length for the boundary conditions, introducing all calibrated boundaries as consistently as possible would result in a nearly closed system, which we can clearly reject with each of the pumping tests type curves. Thus, we conclude that several of the calibrated boundary conditions are the result of overfitting and only some boundary conditions exist in the formation.

One of these boundaries exists between Ktzi 202 and the other two observation wells. From the geological profiles, we know that the aquifer has about double thickness in Ktzi 200 and Ktzi 201 than in Ktzi202 (Figure 1), one part of the aquifer disappears in between. This is a partial boundary, and could explain the type curve for Ktzi 200 (Figure 4). For Ktzi 202, we do not see a boundary, and for Ktzi 201, we observed only one boundary in addition to the partial boundary. However, with a configuration of narrow channels, more boundaries would be observed with the type curves. We conclude that if the aquifer is made up of non-interconnected channels, they have a width of at least 400 m to 600 m, as deduced from the radius of investigation. Nevertheless, if narrower channels exist, and are vertically stacked with interconnections at the contact areas, the pumping test reaction of the flow field may also match our hydraulic observations.

The Horner method (Horner 1951) was applied to calibrate the equilibrium pressure; depending on the borehole and model configuration the values are between 62.5 bara (absolute pressure in bar) and 63 bara for a reference depth of 642 m.

3.2 Early pressure response

The initial pressure response was modelled at the beginning of the drawdown, when the hydraulic head was at equilibrium. It was not modelled for the maximum drawdown when the pumps are switched off, because heterogeneities have a larger impact when the hydraulic pressure is not at a quasi-stationary condition. Furthermore, if the aquifer parameters differ between calibration with early pressure and entire build-up phase, the calibrated drawdown curves are not matched. Thus, the slope during the initial build-up phase cannot be modelled. The difference is caused by a spatially heterogeneous conductivity field, which cannot be implemented with the present approach.

3.3 Cross-hole observations

3.3.1 General overview

For each cross-hole test, the following parameters were fitted: permeability (based on transmissivity) storativity, equilibrated formation pressure and boundary parameters. The first two parameters are presented in Table 4. The information was evaluated with two different methods: (i) the pressure response match of the build-up phase; and (ii) the fit of the initial pressure response. The differences are illustrated by the pressure response in the observation well Ktzi 201 to pumping in Ktzi 202, where the permeability calibrated with the first method is almost twice as that with the second method (Table 4).

Calibrating the parameters to the build-up phase results in a very close fit to both, the drawdown and build-up pressure (Figure 8). However, a closer look at the beginning of the drawdown still reveals a considerable difference between the observed and fitted pressure (Figure 9). It is not surprising that a calibration to the first three hours results in a much closer fit for the respective period, as well for the pressure as for the pressure derivation (Figure 9). However, it is important that the calibrated aquifer parameters are considerably different. This difference can be explained with Figure 3: while the absolute sensitivity is very low at the beginning of the test (Figure 3a), it increases rapidly with time (Figure 3b and Figure 3c). By selective calibration to the first reaction, we can overcome the high (absolute) sensitivity that occurs later in the test, masking the information from the first response. This allows us to focus on the region between the wells, which obviously has a much lower permeability than the adjacent aquifer.

Although the cross-hole values calibrated with the entire build-up phase are sensitive to a larger area than the single-hole tests, the derived transmissivity does not represent a mean for the aquifer (Leven et al. 2006). Due to the alternating sensitivity (Figure 3), results are highly non-unique and obviously differ strongly from the mean value. These values can be only interpreted with a comparison of the results of the initial response. A realistic effective transmissivity is provided by the single-hole results (Desbarats 1994).

Comparing the values which calibrated with the entire build-up phase to those of the early pressure response, the aquifer parameters vary less than 15% for three of six cross-hole combinations. This suggests that the areas between and immediately behind both wells have similar mean characteristics to the lateral and more distant areas (see Figure 3).

For the two cross-hole tests involving observation well Ktzi 201, a satisfying fit is not achievable for the entire build-up phase and homogeneous transmissivity, indicating the presence of a heterogeneity or boundary in the vicinity of Ktzi 201. For other combinations, however, the observed pressures can be fitted with and without boundary configuration. As expected, calibrating the permeabilities to data from the entire build-up phase with boundary configuration results in values roughly twice as high as that without boundaries. For the initial pressure response, only boundaries that are close to either well affect the calibration result. During the pumping test in Ktzi 201, the maximum drawdowns in Ktzi 200 and Ktzi 202 are about 10 and 85 kPa, respectively. In comparison, during pumping in Ktzi 200, the maximum drawdowns in Ktzi 201 and Ktzi 202 are about 55 and120 kPa, respectively. Therefore, the drawdown reactions between Ktzi 200 and Ktzi 201 are smaller than the reaction in Ktzi 202 to pumping in either well. This may be seen as an indication that an impermeable region exists between both wells. However, we can constrain the aquifer geometry by considering the pressure response arrival time: between Ktzi 200 and Ktzi 201, the response of the temporal pressure derivation dp/dt takes about 12 minutes in both directions, whereas it takes about one hour between Ktzi 202 and Ktzi 200 or Ktzi 201 (Table 4). Taking into account that the pressure arrival time is proportional to the square root of the distance (Eq. (3)), the response times of the pressure correspond with the distance between the wells. This shows that a large scale no-flow boundary cannot exist between Ktzi 200 and Ktzi 201.

3.3.2 Anomaly between Ktzi 200 and Ktzi 201

Though the distance between Ktzi 200 and Ktzi 201 is less than or equal to half of any other inter-well distance, the mutual drawdown between these wells is significantly lower than for any other combination. Furthermore, the cross-hole tests in both directions between Ktzi 200 and Ktzi 201 show significantly increased transmissivity and storativity. Thus, it can be concluded that a heterogeneity exists between both wells.

For the pumping test in Ktzi 201, the storativity is independent of the calibration method and about 10^{-3} [-]. In the reverse direction, the storativity is $4.8 \bullet 10^{-4}$ [-] when calibrated with the pressure buildup and $1.7 \bullet 10^{-4}$ [-] when calibrated with the initial response (Table 1). With the exception of the last value, these appear too high to be directly explained by storativity. Hart and Wang (1995) found that the poro-elastic properties of Berea Sandstone vary by ±20%. In comparison, Xu (2007) determined the undrained compressibility of 17 predominantly-sandstone samples from different localities with a broad range of permeability, of which 15 had values between 9 and 14 10^{-11} Pa^{-1}.

The high storage coefficients may be an indication of contact with another aquifer layer and thus a water source between the wells, or they may be the result of vertical cross-flow in the observation wells. In this case, however, they are probably the result of overfitting due to unresolved spatial heterogeneity (Li et al. 2007).

The permeability between Ktzi 200 and Ktzi 201 shows values between 166 and 431 mD, which is significantly greater than the mean aquifer permeability. Due to the alternating sign of spatial sensitivity, two explanations are possible: this may be a virtual effect due to a leaky flow barrier, but it is more likely that a zone of high transmissivity exists, because the calibration of the initial pressure consistently shows a higher permeability.

However, regarding the single-hole evaluation, we do not see any indication of a zone with high permeability, because the wellbore storage masks aquifer effects in the vicinity of the wells up to 50 m (the distance between the two wells). As suggested by the radial mean information about the aquifer provided by the single-hole tests, high permeability in one direction may be counterbalanced by low permeability in another.

3.3.3 Anomaly between Ktzi 201 and Ktzi 202

Calibrating the permeability from the pumping test in Ktzi 202 during pumping in Ktzi 201, we see the opposite transmissivity effect as compared to the tests in Ktzi 200 and Ktzi 201. Transmissivities are lower for the initial pressure response than for the entire build-up phase fit, suggesting a region with lower transmissivity between both wells. The effect is less pronounced for the pumping test in Ktzi 202. A realistic storage coefficient for all combinations does not indicate anomalies or overfitting in this case.

3.4 Permeability discrepancy with respect to core values

The permeability of a horizontally stratified medium determined with pumping tests and slug tests should be similar to the arithmetic mean of core permeabilities (Javandel and Whitherspoon 1969, Butler et al. 1994). Surprisingly, the single-hole tests and many of the cross-hole tests (Table 4) show permeabilities of about one order of magnitude lower than those measured in the core samples (Table 1). In Ktzi 201, the permeability is determined with NMR logs and is very similar to core values (Figure 1). In some parts of the boreholes, the NMR and Coates permeability logs (Coates et al. 1991) show peaks. These can often be attributed to borehole breakout, as indicated by the calibre logs (Figure 1). The discrepancy is not a systematic effect from core expansion. Compared to atmospheric pressure, a confining pressure between 50 and 85 bar does not affect the results (Norden et al. 2010). We therefore conclude that the discrepancy is not a measurement error.

Further, the discrepancy is not a statistical effect. The cores of all three boreholes have mean permeabilities about one order of magnitude higher than the corresponding pumping tests, and the variability of the high permeable parts is low (Figure 1). A re-inspection of the cores revealed that one core segment of about 10 cm length in both Ktzi 201 and Ktzi 202 shows a vertical cementation band (Norden 2007, Fischer personal communication).

In contrast, several authors have reported large-scale permeabilities to be higher than the values derived from core samples (e.g. Hart et al. 2006, Worthington 1977, Urban and Gburek 1988). They attributed the behaviour to fractures in the porous media. In a geostatistical case study, Desbarats (1994) observed that the estimated permeability value is larger than the core permeability. Pavelic et al. (2006) found core values to be 50 times lower than field permeabilities, which they concluded to be due to the small observation scale and the fact that well-cemented cores can be sampled more easily. Raghavan (2004) claimed that pressure tests always yield larger permeabilities than cores, but that the apparent transmissivity of single well tests always decreases with the radius of influence. On the other hand, for fine to coarse sandstones, Runkel et al. (2006) did not observe a systematic deviation between a large number of permeabilities determined by hydraulic tests and core observations. No previous observations of significantly lower permeabilities in pumping tests than in cores have been found.

This discrepancy implies that the primary sandstone layers are not continuous, but that some kind of continuous low-permeability structure exists. In terms of the channel facies, two possibilities exist, singly or in combination. First, when the channels are narrow (about 400 to 600 m or less), they are interconnected and stacked vertically. At their vertical connection, thin layers of silt, mud or strongly-cemented sandstone would lead to a significantly reduced hydraulic connection. Figure 1 illustrates the existence of such layers. In a horizontal setting, these layers do not affect the permeability. Secondly, when the channels are wider than about 400 to 600 m, some kind of continuous vertical (or tilted) structures with low permeability must exist, e.g., cemented fissures or fractures. Core segments with vertical cementations have been found (Norden 2007, Fischer personal communication), which are probably samples from such a structure.

At the Ketzin test site, the maximum slope of the anticline is in the north-northwest direction with a magnitude of about 7.5 degrees (Förster et al. 2006). Considering the resulting shear stress in the vertical direction along the contour lines, this means that the main fissure direction is perpendicular to the maximum slope. This conclusion is consistent with the higher permeabilities found between Ktzi 200 and Ktzi 201 as compared to those between Ktzi 202 and Ktzi 200 or 201.

3.5 Accuracy considerations

The difference between the calibrated initial pressure responses with and without boundaries does not have a physical meaning. It simply reflects the conceptual boundary model. Boundaries have an impact which are more or less perpendicular to the line between the pumping and observation well, and are limited to a location near to either of these wells (cases: Ktzi 200→Ktzi 202, Ktzi 201→Ktzi 201, Ktzi 202→Ktzi 201). If the boundary is parallel to the connecting line between the wells (Ktzi 202→Ktzi 200) or if the distance between boundary and observation well is relatively high (Ktzi 200→Ktzi 201), the calibrated parameters are identical for the initial pressure response and the entire build-up phase.

The wells are connected to several permeable layers with different thicknesses. Indications for vertical cross-flow between the different layers exist from borehole temperatures measured during hydraulic tests in the observation well Ktzi 200 (Henninges, personal communication).Taking into account the layer thickness proportions (see 2.1, Geology and Boreholes), the effect is not considered to be significant.

The reservoir pressure could not be determined directly. Due to the fact that pressure transducers were run into the pumping well along with the pump and tubing, the displacement increased the water table elevation and inhibited the direct determination of reservoir pressure. The pressure transducer in the observation well is located at least 400 m above the filter screen, and a correction of reservoir pressure would require knowledge of the exact density of the fluid between the pressure transducer and the well screen. Due to previous fluid injections, this could not be carried out. The reservoir pressure was therefore a fitting parameter, which was determined indirectly with the Horner method (Horner 1951, Bourdet 2002).

Three pumping events have been carried out for Ktzi 201. Only the third event was analysed, owing to the longer build-up period. The fit for the entire pressure history shows significant deviations in Ktzi 200 for the calibrated period (Figure 7). This shows that either the calibration approach does not sufficiently describe the flow, or that the time after the last pumping test was too short for the system to reach again the hydraulic equilibrium, and probably introduces a bias to the results.
Due to the genesis of the formation, a significant horizontal anisotropy appears to be probable. This may have an impact on the results and may explain some part of the heterogeneity. However, this factor could not be considered with the applied analytical approach.

3.6 Comparison with multiphase modelling

Modelling studies at the Ketzin site, where CO_2 has been injected through Ktzi 201 since the summer of 2008, allow for further assessment of the third aquifer configuration. The arrival time of injected CO_2 in Ktzi 200 can be well predicted with a homogeneous aquifer model (Lengler et al., 2010), or a model which is homogeneous in the near-well area (Kempka et al. 2010). Inserting the second aquifer configuration in these models would substantially increase the arrival time.
The abovementioned multiphase models underestimate the arrival time at Ktzi 202 considerably. The observed time was four times longer than predicted. The third configuration, with reduced permeability between Ktzi 201 and Ktzi 202, can explain this delayed arrival of CO_2 in Ktzi 202. However, although the arrival time at Ktzi 200 is predicted correctly by both homogenous models, it would be underestimated when modelling with the third configuration. Although this is a counter-indication, it is not a reason to reject this configuration, since the models have other degrees of freedom which allow for the calibration of the arrival time.
The single-hole test in Ktzi 201 shows a permeability of 90 mD, which is equal to the value obtained by Lengler et al. (2010) with a history fit of the injection pressure. These authors used a sandstone body thickness of 12 m (compared to 17.6 m used in this study), and applied a relative permeability function. This does not allow a direct comparison, but nevertheless, from a geological perspective, the values are quite similar.

4 Conclusions

We have discussed three different aquifer configurations based on an analytical evaluation of pumping test data. Due to the non-unique character of the results, it is not possible to obtain one definite aquifer configuration. Depending on the context, different configurations appear to be reasonable.
For the first aquifer configuration, we attempted to obtain the best fit by interpreting the data sets independently of each other. Most of the pressure fits are excellent (Figure 4 to Figure 8). This configuration is probably consistent with the modelled arrival time (Kempka et al., 2010), but is probably inconsistent with the pressure history in Ktzi 201. Furthermore, the resulting interpretation of the geology is inconsistent and the anomaly between wells Ktzi 200 and Ktzi 201 cannot be explained.
In the second aquifer configuration, consistent interpretation was possible by introducing a low permeability fracture between these wells (Figure 10). The low permeability fracture explains, in principle, the hydraulic reaction between both observation wells. It is consistent with a single-hole test, suggesting a boundary configuration of one to two boundaries for Ktzi 201. It is also consistent with decreasing permeability and increasing distance for Ktzi 200, and with pressure arrival times. Unfortunately, this configuration cannot be tested because it is not possible to model leaky boundaries analytically in Interpret2006. The second aquifer configuration is quite simple since it requires only a few assumptions. However, the boundary is located too close to the wells to fully explain the type curve data.
The arrival times of injected CO_2 in Ktzi 200 can be well predicted with a homogeneous

aquifer model (Lengler et al., 2010; Kempka et al., 2010). However, the second configuration would substantially increase the arrival time. Further, the reaction of the cross-hole tests, especially the initial reaction, suggests that a zone of high permeability exists between Ktzi 200 and Ktzi 201.

We have therefore developed a third aquifer configuration (Figure 10), which was based on interpretations of the spatial and temporal sensitivities of the tests. In this configuration, Ktzi 200 and Ktzi 201 are located within a zone of high permeability, which is identified by cross-hole observations between the wells. It was not detected with the single-hole tests, we assume due to the wellbore storage effect and well skin, and mitigation by anisotropy. Around this zone, regions with low permeabilities exist.

The results of CO_2 injection models support the third aquifer configuration. One model is homogeneous (Lengler et al., 2010), and three models are homogenous in the near-well area (which includes Ktzi 202, Kempka et al., 2010). All models underestimate the arrival of CO_2 in Ktzi 202 by a factor of ~4, for which the zone of reduced permeability between Ktzi 201 and Ktzi 202 is a reasonable explanation. Lengler et al. (2010) calibrated an aquifer permeability of 90 mD with the CO_2 injection pressure history, which is equal to the value obtained from the single-hole test in Ktzi 201. Due to methodical differences, the numbers are not directly transferable, but the values are nevertheless very similar from a geological perspective.

Considering that core permeabilities are one order of magnitude higher than pumping test permeabilities, we conclude that the latter values are clearly more representative of injection behaviour and allow for a better prediction.

The fact that core permeabilities are much higher than pumping test values is very unusual and has not been reported elsewhere in the literature; it appears to be a unique feature of the field site. It also implies that the sandstone body is not continuous, but intersected by continuous low-permeability layers or regions. When the channels are narrow (smaller than about 400 to 600 m), these are interconnected and stacked vertically. When the channels are wide (larger than about 400 to 600 m), then they must have vertical structures of low permeability, e.g., cemented fractures. Two core sections show such structures.

Due to the experimental set up and the geological situation, the data as well as the evaluation bear some degree of ambiguity and inaccuracy. This may bias the results, but it is not thought to affect the general process description.

Acknowledgements

We thank Stephan Rohs (Golder Asscociates), Thomas Wöhrl (GFZ) and Fabian Möller (GFZ), and Jochen Zemke (UGS) for the planning and operation of the tests. We also thank Ben Norden (GFZ) and Andrea Förster (GFZ) for providing the geological background and fruitful discussions. Special thanks are given to Kirsten Rempel (GFZ) for revision.

We acknowledge the suggestions of the two anonymous reviewers. The CO_2SINK project received its funding from the European Commission FP6, the Federal Ministry of Economics and Technology BMWi, the Federal Ministry of Education and Research BMBF and industry partners.

5 References

Bourdet, D., 2002. Well Test Analysis: The Use of Advanced Interpretation Models. Elsevier Science B.V.

Butler, J., Bohling, G., Hyder, Z., Mcelwee, C., 1994. The use of slug tests to describe vertical variations in hydraulic conductivity. Journal of Hydrology 156 (1-4), 137-162.

Coates, G. R., Peveraro, R., Hardwick, A., Roberts, D., 1991. The magnetic resonance imaging log characterized by comparison with petrophysical properties and laboratory core data. Proceedings of the 66th Annual Technical Conference and Exhibition, Formation Evaluation and Reservoir Geology, SPE 22723, 627–635.

Daungkaew, S., Hollaender, F., Gringarten, A., 2000. Frequently Asked Questions in Well Test Analysis. SPE Annual Technical Conference and Exhibition, 1-4 October 2000, Dallas, Texas. SPE 63077, 14p.

Desbarats, A. J., 1994. Spatial Averaging Of Hydraulic Conductivity Under Radial Flow Conditions. Mathematical Geology 26 (1), 1-21.

Enachescu, C., Frieg, B., Wozniewicz, J., 2004. A new visual tool for transient test data. NGWA Conference, Portland Maine September 13 to 15, Golder Associates and NAGRA. 12p.

Frykman, P., Zink-Jørgensen, K., Bech, N., Norden, B., Förster, A., Larsen, M., 2006. Site characterization of fluvial, incised-valley deposits. In Proceedings, CO2SC Symposium, Lawrence Berkeley National Laboratory 2006.

Förster, A., Norden, B., Zinck-Jørgensen, K., Frykman, P., Kulenkampff, J., Spangenberg, E., Erzinger, J., Zimmer, M., Kopp, J., Borm, G., Juhlin, C., Cosma, C.-G., Hurter, S., 2006. Baseline characterization of the CO2SINK geological storage site at Ketzin, Germany. Environmental Geosciences 13 (3), 145-161.

Förster, A., Schöner, R., Förster, H.-J., Norden, B., Blaschke, A.-W., Luckert, J., Beutler, G., Gaupp, R., Rhede, D. The Upper Triassic Stuttgart Formation (Middle Keuper) at Ketzin: The reservoir for pilot CO2 storgae in the Northeast German Basin. submitted to Marine and Petroleum Geology.

Fischer, S., images of core samples from observation well CO2 Ktzi 200/2007, personal communication

Hart, D., Bradbury, K., Feinstein, D., 2006. The vertical hydraulic conductivity of an aquitard at two spatial scales. Ground Water 44 (2), 201-211.

Hart, D. Wang, H., 1995. Laboratory Measurements Of a Complete Set of Poroelastic Moduli for Berea Sandstone and Indiana Limestone. Journal Of Geophysical Research-Solid Earth 100 (B9), 17741-17751.

Horner, D., 1951. Pressure Build-up in Wells. in 3rd World Petroleum Congress, May 28 - June 6, The Hague, Netherlands.

Javandel, I. Witherspoon, P. A., 1969. A Method of Analyzing Transient Fluid Flow in Multilayered Aquifers. Water Resour. Res. 5, 856-869.

Juhlin, C., Giese, R., Zinck-Jørgensen, K., Cosma, C., Kazemeini, H., Juhojuntti, N., Lüth, S., Norden, B., Förster, A., 2007. Case History - 3D baseline seismics at Ketzin, Germany: The CO2SINK project. Geophysics 72, 121-132.

Kempka, T., Kühn, M., Class, H., Frykman, P., Kopp, A., Nielsen, C., Probst, P., CO2Sink Group, 2010. Predictive Modelling of Ketzin - CO2 arrival in the observation well.

International Journal of Greenhouse Gas Control.

Lengler, U., De Lucia, M., Kühn, M., CO2Sink Group, 2010. The impact of heterogeneity on the distribution of CO2: Numerical simulation of CO2 storage at Ketzin. International Journal of Greenhouse Gas Control.

Leven, C. Dietrich, P., 2006. What information can we get from pumping tests?-comparing pumping test configurations using sensitivity coefficients. Journal of Hydrology 319 (1-4), 199-215.

Li, W., Englert, A., Cirpka, O. A., Vanderborght, J., Vereecken, H., 2007. Two-dimensional characterization of hydraulic heterogeneity by multiple pumping tests. Water Resour. Res. 43, 13p.

Norden, B., 2007. Geology of Ketzin. (Workpackage 7.2) .CO2Sink 9th Project Meeting.

Norden, B., Förster, A., Vu-Hoang, D., Marcelis, F., Springer, N., Le Nir, I., 2010. Lithological and Petrophysical Core-Log Interpretation in the CO2SINK, the European CO2 Onshore Research Storage and Verification Project. SPE Reservoir Evaluation & Engineering.

Paradigm, 2006. Interpret2006 - Well Test Analysis Software. Paradigm Ltd.

Pavelic, P., Dillon, P., Simmons, C., 2006. Multiscale characterization of a heterogeneous aquifer using an ASR operation. Ground Water 44 (2), 155-164.

Prevedel, B., Wohlgemuth, L., Henninges, J., Krüger, K., Norden, B., Förster, A., CO2SINK Drilling Group, 2008. The CO2SINK boreholes for geological storage testing. Scientific Drilling 6, 32-37.

Raghavan, R., 2004. A review of applications to constrain pumping test responses to improve on geological description and uncertainty. Rev. Geophys. 42, 29p.

Renard, P., Gomez-Hernandez, J., Ezzedine, S., 2006. Characterization of Porous and Fractured Media. Encyclopedia of Hydrological Sciences, John Wiley & Sons, Ltd. (147), 1-18.

Runkel, A., Tipping, R., Alexander, E., Alexander, S., 2006. Hydrostratigraphic characterization of intergranular and secondary porosity in part of the Cambrian sandstone aquifer system of the cratonic interior of North America: Improving predictability of hydrogeologic properties. Sedimentary Geology 184 (3-4), 281-304.

Streltsova, T., 1987. Well testing in heterogeneous formations., John Wiley and Sons Inc. New York, USA.

Urban, J. Gburek, W., 1988. Determination of Aquifer Parameters at a Ground-Water Recharge Site. Ground Water 26 (1), 39-53.

Vasco, D. Karasaki, K., 2001. Inversion of pressure observations: an integral formulation. Journal of Hydrology 253, 27-40.

Vasco, D. W., Keers, H., Karasaki, K., 2000. Estimation of reservoir properties using transient pressure data: An asymptotic approach. Water Ressources Research 36, 3447-3465.

Wiese, B. Nützmann, G., 2008. Inverse Modelling of Aquitard Structures Using Pilot Points and Regularisation., IAHS Redbook 320, pp. 272-277.

Worthington, P. F., 1977. Permeation properties of the Bunter Sandstone of northwest Lancashire, England. Journal of Hydrology 32 (3-4), 295-303.

Würdemann, H., Möller, F., Kühn, M., Heidug, W., Christensen, N.P., Borm, G., Schilling, F. 2010. CO2SINK – From Site Characterisation and Risk Assessment to Monitoring and Verification: One Year of Operational Experience with the Field Laboratory for CO2 Storage at Ketzin, Germany. International Journal of Greenhouse Gas Control.

Xu, C., 2007. Estimation of Effective Compressibility and Permeability of Porous Materials with Differential Acoustic Resonance Spectroscopy. PhD thesis, Department of Geophysics, Stanford University.

Zambrano, J., Zimmermann, R., Gringarten, A., 2000. Influence of Geological Features on Well Test Behaviour - SPE 59398. SPE Asia Pacific Conference, Yokohama, Japan 25-26 April 2000.

Zettlitzer, M., Moeller, F., Morozova, D., Lokayc, P., Würdemann, H., CO2SINK Group, 2010. Re-Establishment of the Proper Injectivity of the CO2-Injection Well Ktzi201 in Ketzin, Germany. International Journal of Greenhouse Gas control.

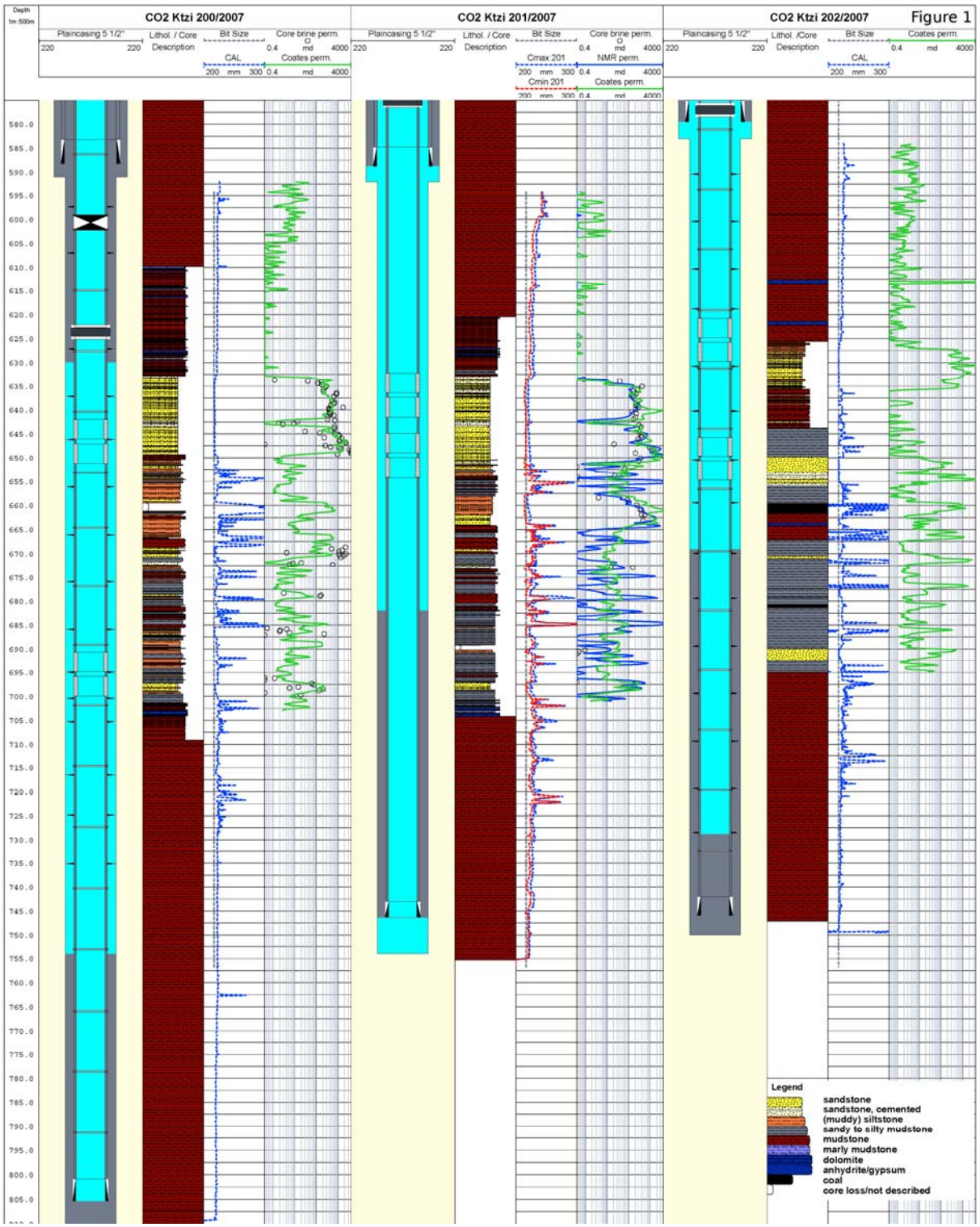

Figure 1: Profiles of the wells Ktzi 200, Ktzi 201 and Ktzi 202. The first column shows the borehole completion (after Prevedel et al., 2008) with the consolidated casing cements in gray and the annular space of partly-consolidated cement represented by cross-hatching. The circles represent values which are determined with core samples, the green line represents the Coates permeability, and the blue line represents the NMR permeability. The second column is the geological profile (Förster et al. submitted), the third column presents the caliber log, and the fourth column shows the measured permeabilities (Norden et al. 2010).

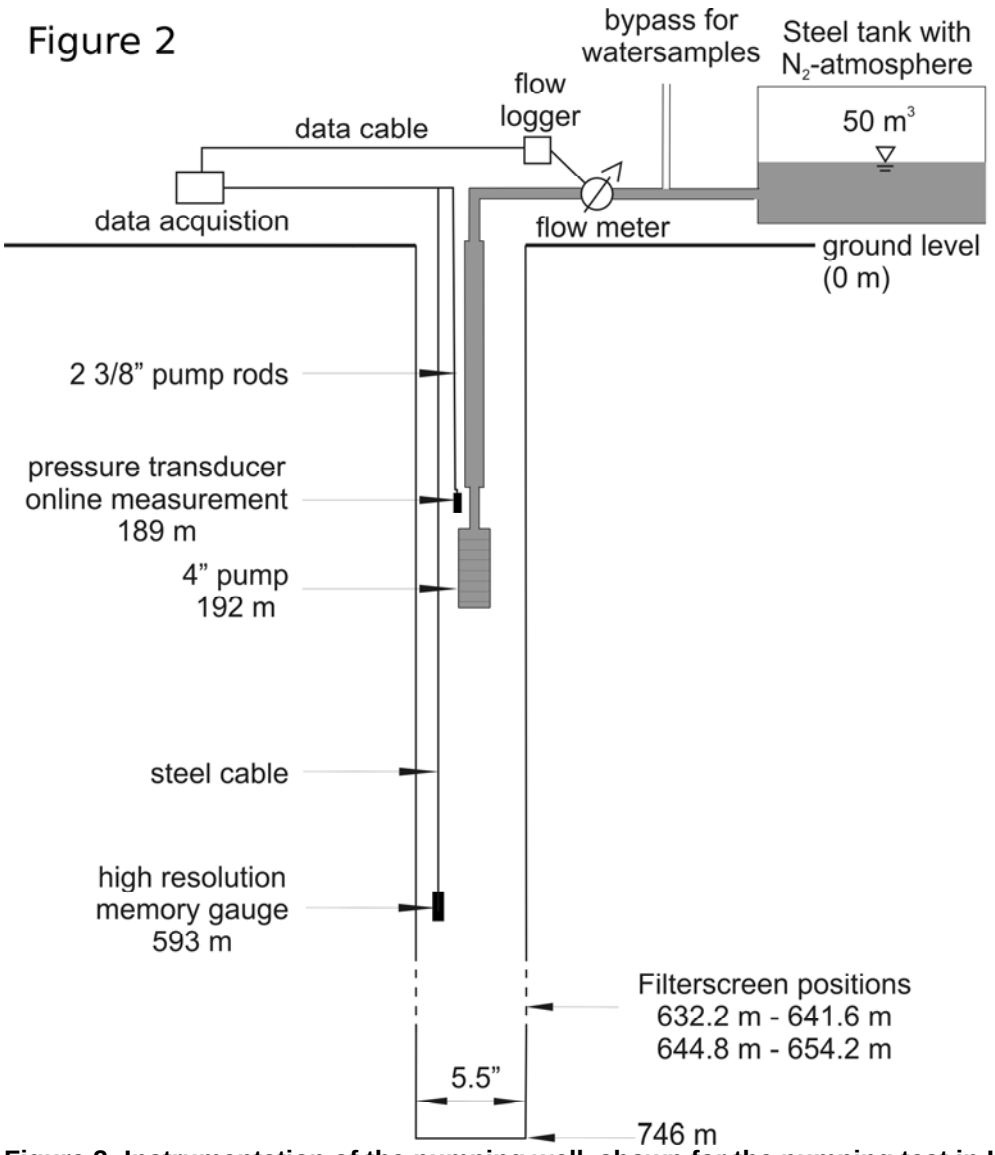

Figure 2: Instrumentation of the pumping well, shown for the pumping test in Ktzi 201.

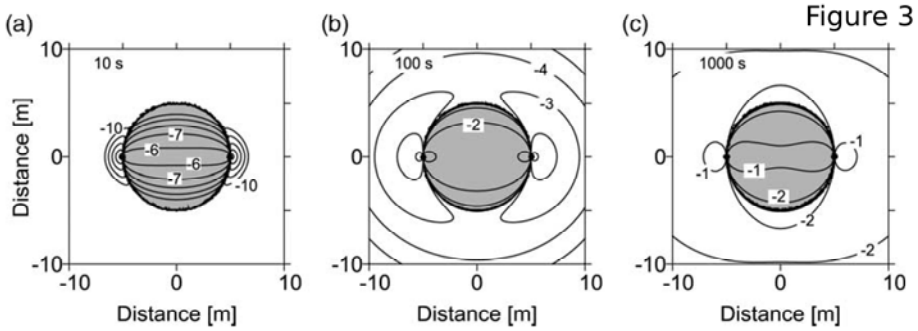

Figure 3: Distribution of the logarithm of the sensitivity with respect to transmissivity for a homogeneous aquifer based on the Theis solution. The zone with grey background has positive sensitivity (log10(l)), and the surrounding zone has negative sensitivity with respect to transmissivity (log10(-l)). The wells are located at (5/0) and (-5/0), respectively. Figure and caption from Leven et al. (2006).

Figure 4

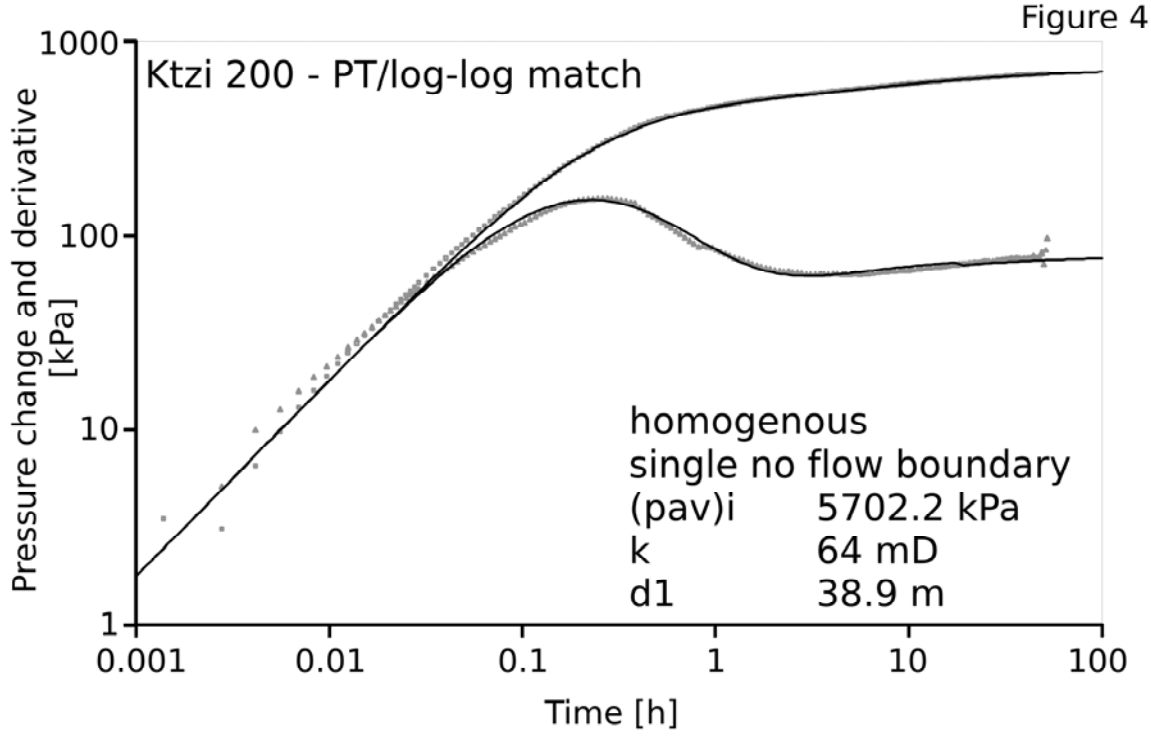

Figure 4: Type curve and interpretation for well Ktzi 200. The x-axis shows the time, and the y axis shows the pressure change and derivative of pressure change. The upper curve corresponds to the pressure change, and the lower curve corresponds to the derivative.

Figure 5

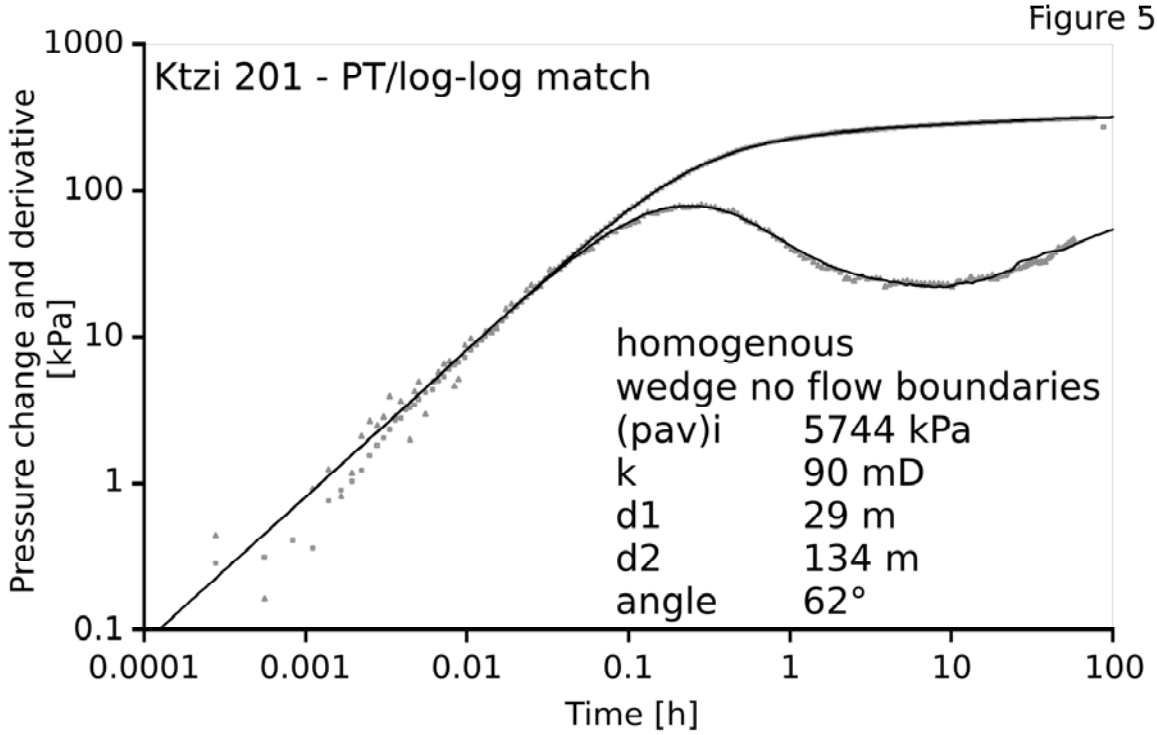

Figure 5: Type curve and interpretation of the first pumping test in well Ktzi 201. The x-axis shows the time, and the y axis shows the pressure change and derivative of pressure change. The upper curve corresponds to the pressure change, and the lower curve corresponds to the derivative.

Figure 6

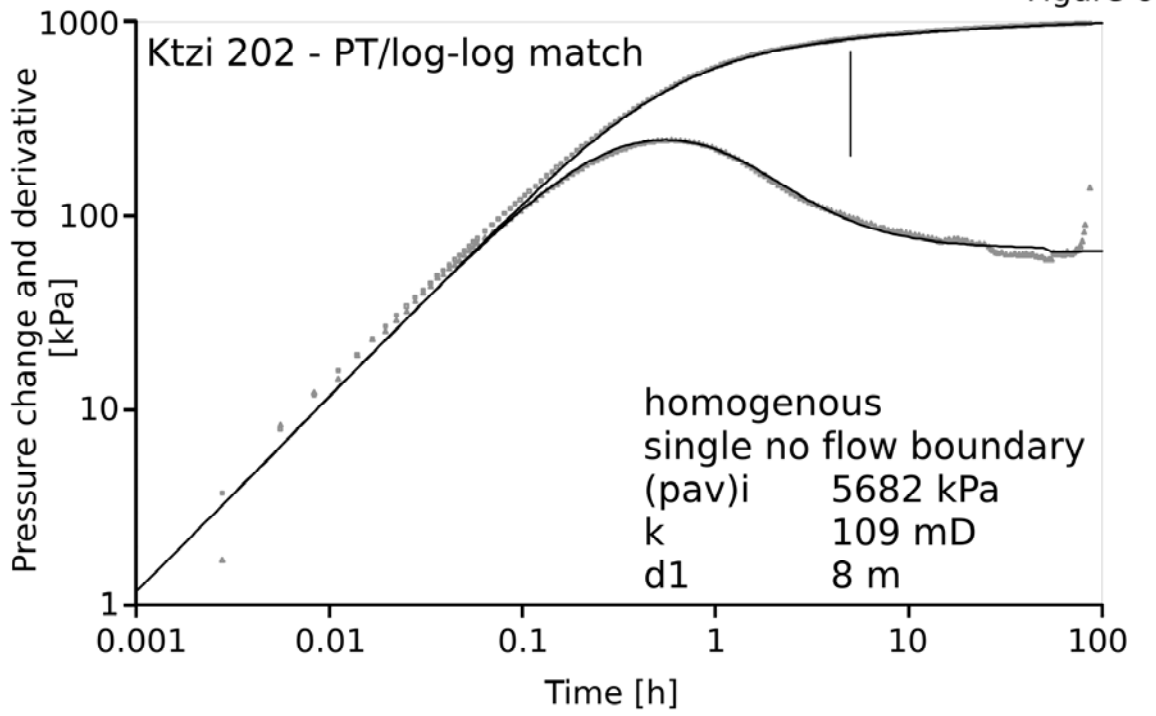

Figure 6: Type curve and interpretation of well Ktzi 202. The x-axis shows the time, and the y axis shows the pressure change and derivative of pressure change. The upper curve corresponds to the pressure change, and the lower curve corresponds to the derivative.

Figure 7

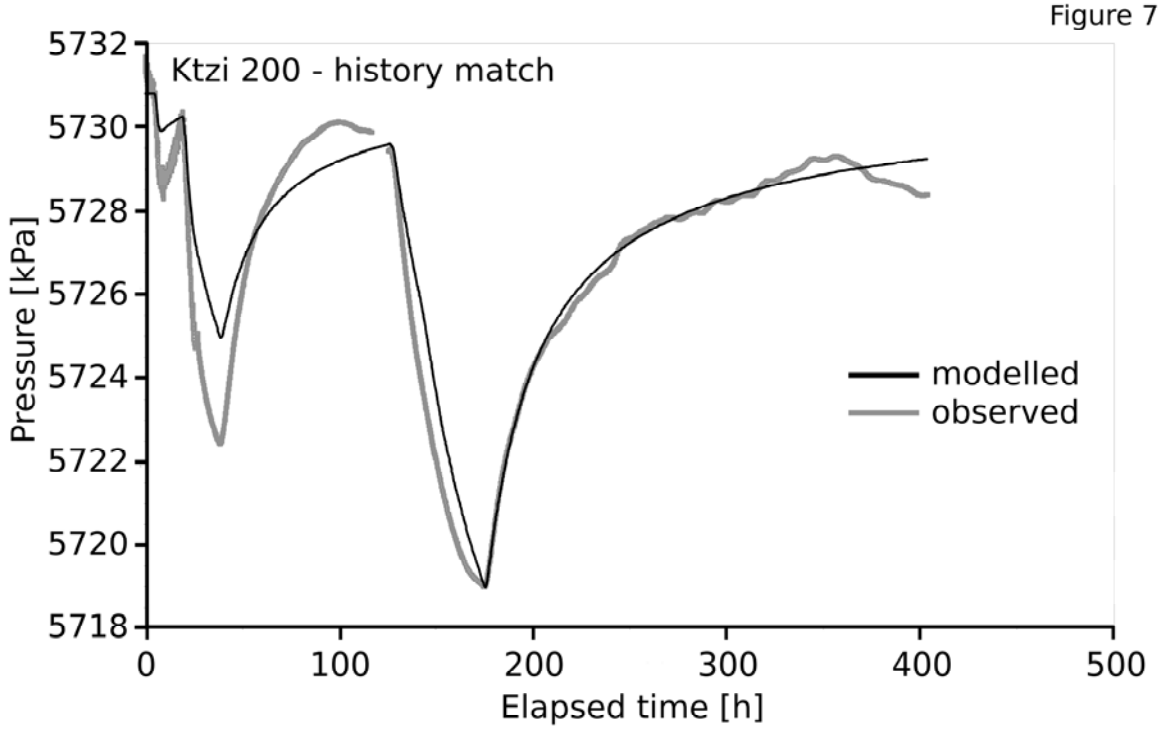

Figure 7: Pressure fit in observation well Ktzi 200 for the pumping test in Ktzi 201. The grey curve represents observed data, and the black curve shows simulated values. The parameters were fitted to the last drawdown and build-up. The fluctuating pressure after 220 hours was caused by a slug test in Ktzi 201.

Figure 8

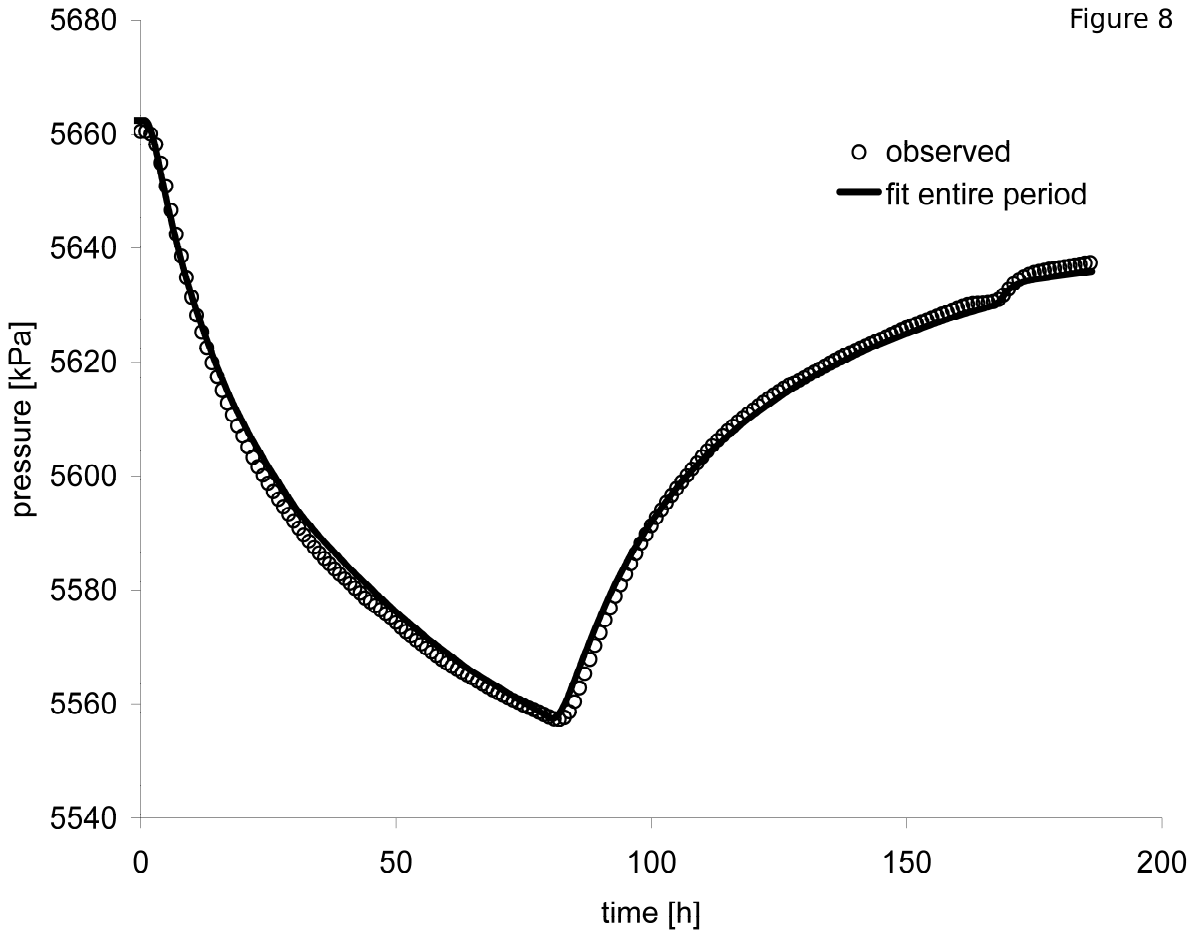

Figure 8: Drawdown of simulated and observed pressure response for the pumping test in Ktzi 202 with observation in Ktzi 201. The black line refers to the best fit for the entire build-up phase, and the black circles show observed values. The deviation at 170 hours was caused by a slug test in Ktzi 201. The first three hours are presented in Figure 9.

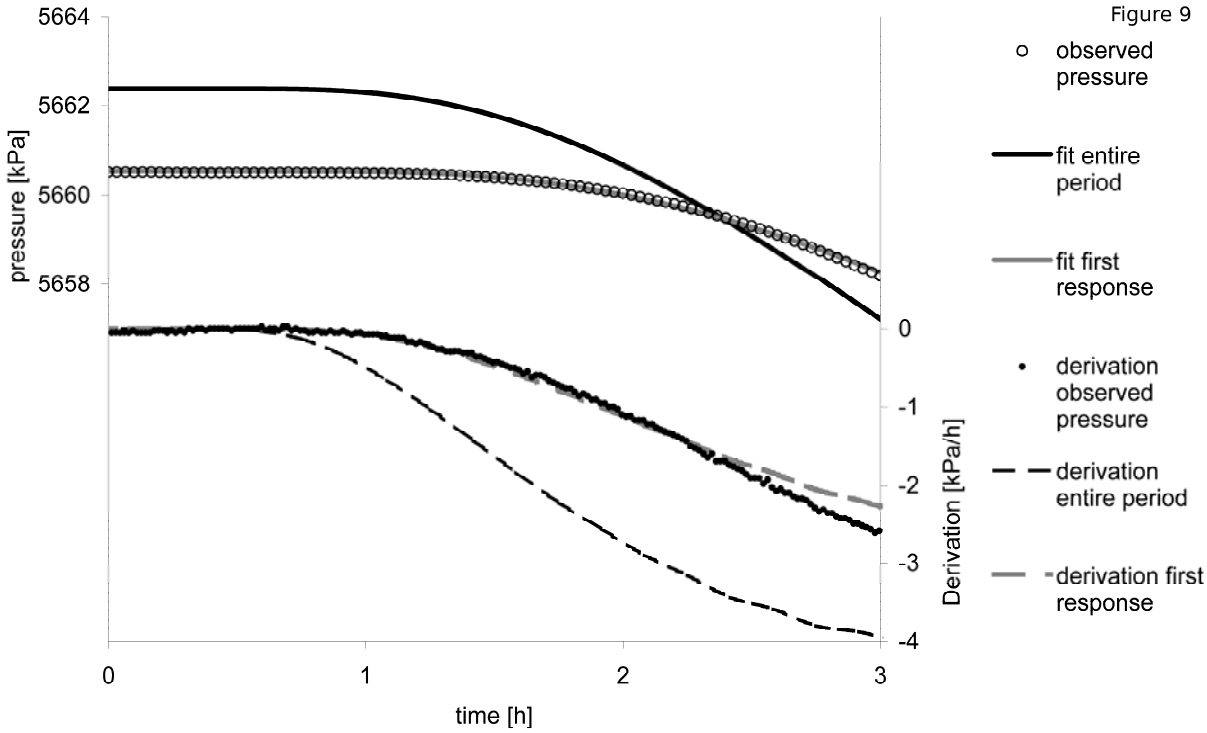

Figure 9: Drawdown and first temporal derivative of simulated and observed pressure response for the pumping test in Ktzi 202 with observation in Ktzi 201. The data is identical to the initial phase of Figure 8. The upper lines refer to the left axis, and the lower lines refer to the right axis. The curves for the first response (grey curves) are, for the most part, identical with the observed data. The calibrated parameters are presented in Table 4.

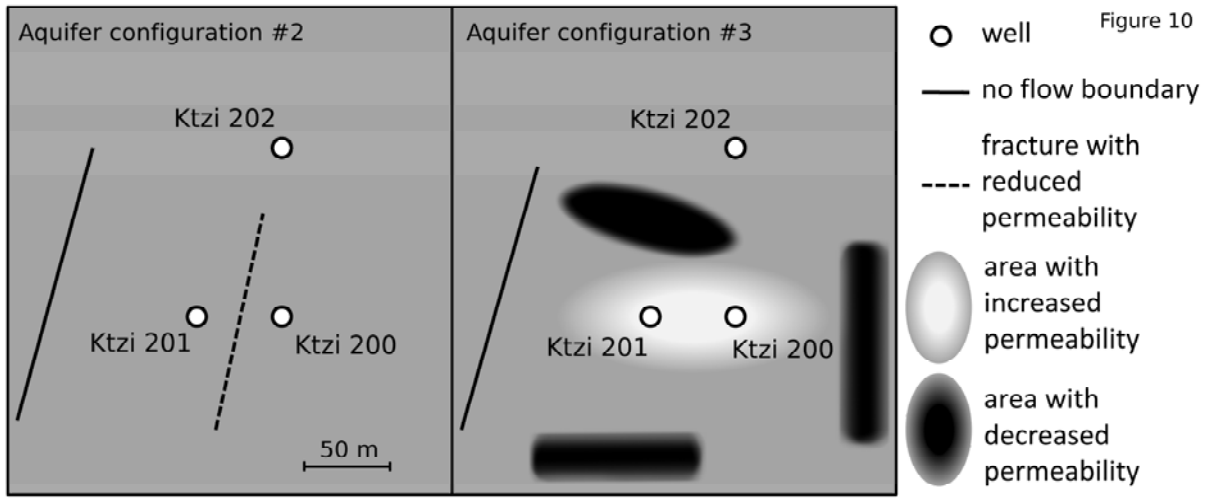

Figure 10: Two aquifer configurations considered in this study. The left configuration includes a rather homogeneous distribution of permeability and a low-permeability fracture between Ktzi 200 and Ktzi 201. The right configuration assumes a zone of increased transmissivity between Ktzi 201 and Ktzi 200, and a zone of reduced permeability between Ktzi 201 and Ktzi 202. The position of these zones (oval shape) is known approximately. Indications for zones of reduced permeability exist near Ktzi 200 and Ktzi 201, shown as dark, elongate areas. An impermeable boundary appears to exist near Ktzi 201. The positions of the rectangular zones and the impermeable boundary are illustrative and not known. The quality of the configurations is assessed in Table 5.

1 Tables

Table 1: Measured mean permeability and aquifer thickness (Norden et al. 2010). For Ktzi 200 and Ktzi 201, permeabilities were determined using core samples; for Ktzi 201, permeabilities were determined from borehole logging data using the Coates equation (Coates et al. 1991). Samples with a permeability >= 100 mD are considered to be aquifer samples.

Borehole	Layer	Permeability [mD]	Thickness [m]	Transmissivity [mD*m]
Ktzi 200	#1	617	8.5	5242
	#2	1787	6.1	10903
	total	1106	14.6	16145
Ktzi 201	#1	348	8.5	2959
	#2	673	8.7	5829
	#3	566	5.1	2887
	total (1+2)	512	17.2	8788
Ktzi 202*	total	805	8	6440

Table 2: Evaluated aquifer tests. Start and end dates refer to the entire build-up phase, including the drawdown and build-up periods, while the average rate refers only to the pumping period.

Start	End	Type	Well	Volume [m³]	Average rate [m³/h]
14-Sep-07	27-Sep-07	2 Production Tests	Ktzi 201	71	1.1
01-Oct-07	05-Oct-07	1 Production Test	Ktzi 200	72	1.8
07-Jan-08	14-Jan-08	1 Production Test	Kzti 202	92	1.2

Table 3: Calibrated location of the no-flow boundaries and the corresponding well parameters (skin and wellbore storage). The slash indicates a configuration with and without boundary condition. NA: not applicable.

Observation well	Pumping well	No. of Boundaries	Distance from Ktzi 200	Distance from Ktzi 201	Distance from Ktzi 202	Skin	Wellbore storage
200	200	1	39	NA	NA	0.54	9.70E-04
	201	1	52	52	148	NA	NA
	202	1	29	78	10	NA	NA
201	200	1	43	88	85	NA	NA
	201	2	NA	#1:29, #2:139	NA	2.7	9.60E-04
	202	1	79	95	11	NA	NA
202	200	1	39	8	6	NA	NA
	201	1	55	10	10	NA	NA
	202	1/0	NA	NA	8/-	5/0.3	8.8e-4/8.6e-4

Table 4: Calibrated aquifer parameters for single-hole and cross-hole evaluations. For the former, the aquifer thickness is identical to the observed thickness; for the latter, the thickness is the mean of the observed thickness in both wells. Configurations exist where the fit for the entire build-up phase and the fit for the initial pressure response differ considerably (15% or more); these are shaded grey. An asterisk (*) indicates an increased deviation of the pressure fit. The response time was determined as the first reaction of the first pressure derivative. NA: not applicable.

Observation well	Pumping well	Mean aquifer thickness	Boundary configuration						No boundaries						Response time
			entire build-up phase			initial response			entire build-up phase			initial response			
Ktzi	Ktzi	[m]	[mD*m]	[mD]	s[-]	[mD*m]	[mD]	s[-]	[mD*m]	[mD]	s[-]	[mD*m]	[mD]	s[-]	[min]
200	200	14.6	914	63	NA		NA		600*	41*	NA		NA		NA
	201	16.1	6396*	397*	1.3e-3*	6933	431	1.0E-3	no satisfying fit			4409	274	8.9E-4	12
	202	11.3	1267	112	9.2E-5	1145	101	1.1E-4	636	56	4.8E-5	581	51	5.8E-5	59
201	200	16.1	2668	166	4.8E-4	3156	196	1.7E-4	no satisfying fit			3080	191	1.6E-4	11
	201	17.6	1576	90	NA		NA		no satisfying fit				NA		NA
	202	12.8	1280	100	7.0E-5	700	55	5.9E-5	641	50	3.9E-5	397	31	3.6E-5	84
202	200	11.3	1130	100	9.1E-5	1108	98	9.6E-5	570	50	4.8E-5	564	50	5.1E-5	57
	201	12.8	874	68	7.0E-5	701	55	6.7E-5	377	29	3.9E-5	350	27	3.4E-5	50
	202	8	873	109	NA		NA		432	54	NA		NA		NA

Table 5: Multi-criteria comparison of the three configurations. Configurations #2 and #3 are presented in Figure 10. The symbols represent the relative fulfilment of a criterion with respect to the other models. Legend: "+" = best, "o" = medium, and "-" = worst.

Criteria	Aquifer configuration #1 (Multi boundary approach)	Aquifer configuration #2	Aquifer configuration #3
Fit to single-hole tests	+	+/assumed	assumed
Fit to cross-hole tests	+	assumed	assumed
Consistency of hydraulic interpretation	-	o	+
Simplicity of aquifer configuration	o	+	-
Agreement with core permeabilities	-	-	+
Agreement with permeabilities of CO_2 injection model (Lengler et al. 2010)	o	o	o/+
Agreement with hydrogeological configuration of CO_2 model (Frykman 2006)	o	-	+